Engineered Science
DOI: https://dx.doi.org/10.30919/es1760

High-performance and Energy-saving Tire Tread Rubber Achieved Through Synergistic Charge Regulation and Flexible Bridging Interface

Shuaishuai Cheng,* Bo Xu, Xiaoyuan Duan and Yaqing Liu*

Abstract

The automotive tire industry faces mounting environmental challenges as a significant contributor to global energy consumption and emissions. Addressing this requires high-performance eco-friendly tire materials, where uniform nanofiller dispersion and robust rubber-filler interfaces remain critical hurdles. This study developed a dual-enhancement strategy through charge regulation and flexible interfacial bridging to fabricate advanced natural rubber (NR) composites. Positively charged graphene oxide (PGO) was synthesized via electrostatic self-assembly using biocompatible polydiallyldimethylammonium chloride (PDDA) as an interfacial modifier. The NR/PGO composites were subsequently prepared through aqueous-phase co-precipitation and hot-press vulcanization. Electrostatic attraction between cationic PGO and anionic NR latex enabled exceptional filler dispersion without density-driven stratification. Simultaneously, non-polar PDDA chains formed flexible bridges with NR molecules, synergistically strengthening interfacial interactions. This dual mechanism yielded NR/PGO composites with significantly enhanced properties, showed a 14.0% increase in tensile strength to 30.1 MPa and an 19.0% increase in tear strength to 63.9 N/mm compared to NR/GO. Compression fatigue heat buildup decreased by 17.5%, while wear resistance improved by 14.4%. Solid tires fabricated from these composites exhibited 7.3% lower dynamic temperature rise and 13.0% reduced rolling resistance. This work establishes a novel pathway for engineering sustainable, high-performance tire materials.

Keywords: Tread rubber; Electrostatic self-assembly; Flexible bridging interface; Dynamic thermal properties.
Received: 29 July 2025; Revised: 07 September 2025; Accepted: 29 September 2025
Article type: Research article.

1. Introduction

In the context of the continuous deepening of the global green development strategy, the automotive tire industry, as a key area for the transformation of high-energy-consuming industries, faces the dual challenges of improving energy efficiency and controlling environmental pollution.[1–3] As a major source of carbon emissions in the transportation sector, the tire industry urgently needs to achieve the dual goals of energy conservation and performance breakthroughs through material innovation. Natural rubber (NR), with its excellent mechanical properties, electrical insulation characteristics, and unique self-reinforcing ability, has long occupied a core position as the base material for engineering tires. However, its functional realization still heavily relies on the synergistic effect of reinforcing fillers, especially in terms of modulus, tear strength and thermal conductivity improvement.[4,5] Nanoscale fillers such as carbon black, silica, carbon nanotubes, and graphene derivatives exhibit unique size effects.[6–9] As a result, they are widely used in the reinforcement of NR.

Generally, the effective performance of nanofillers in rubber is primarily constrained by the uniformity of dispersion and the interfacial interaction. Graphene oxide (GO), as a functionalized derivative of graphene, possesses theoretical high strength, large specific surface area and abundant active oxygen-containing functional groups.[10–12] It is regarded as one of the most promising rubber reinforcing agents, which is theoretically capable of significantly enhancing the strength, toughness, and wear resistance of rubber composites. Moreover, GO has good dispersibility in aqueous solutions. Therefore, it is often added to NR latex as a reinforcing agent through the latex blending method. However, the dispersed phase of NR in water is different from that of GO. The latex particles of NR exist in the form of a suspension. The

Shanxi Key Laboratory of Nano-functional Composite Materials, North University of China, Taiyuan, 030051, China
*Email: shuaischeng@nuc.edu.cn (S. cheng); lyq@nuc.edu.cn (Y. Liu)

molecular chains of NR have hydrophobic ends consisting of phospholipids and hydrophilic ends consisting of proteins. Additionally, the rubber molecular chains themselves are nonpolar. In contrast, the surface of GO is rich in oxygen-containing functional groups, such as hydroxyl and carboxyl groups, which endow it with strong polarity. This leads to insufficient interfacial compatibility between GO and NR due to the polarity difference, which making it highly prone to agglomeration.[13,14] This severely restricts its application effectiveness in rubber composites. More importantly, when rubber composites are subjected to external forces, these interfacial defects not only reduce the efficiency of stress transfer but also exacerbate energy dissipation under dynamic loads, which in turn triggers a temperature rise within the rubber. This is particularly critical for tread rubber used in tires. High temperatures can deteriorate its mechanical properties and accelerate the thermal degradation of the tread rubber, which posing a serious threat to the service life of tire tread rubber.[15,16] Therefore, it is of great urgency to develop new preparation technologies to enhance the interfacial interaction between GO and NR.

To address the issue of interfacial regulation between GO and NR, researchers have actively explored a variety of modification approaches, striving to optimize the dispersion of GO in rubber and enhance the interfacial bonding with NR. Zhang Liqun and Lu Yonglai team[17–20] enhanced the interfacial interactions between GO and NR by designing molecular chain orientation, employing strain-induced crystallization control techniques characterized by synchrotron radiation wide-angle X-ray diffraction (WAXD) and polarized infrared spectroscopy. Tang Zhenghai and Guo Baochun team[21–24] synergistically improved filler dispersion and interfacial bonding through the combined effects of hydrogen bonding and vulcanization grafting. This was achieved using an in-situ modification technique with protonated ionic liquids bearing functional groups (*e.g.*, hydroxyl, sulfhydryl, and double bonds). Liu[25] and Woraphutthaporn[26] achieved enhanced interfacial interactions between GO sheets and NR particles by using silane coupling agents Si69 and KH550 to covalently modify GO fillers. This significantly improved the mechanical properties of the composites. In addition, some researchers have used the method of loading vulcanization agents onto GO[27–30] to produce rubber composites with improved dispersion and interfacial interactions. These approaches mainly rely on the thiol or sulfur functional groups in the selected modifiers to form chemical bonds with the rubber molecular chains during the vulcanization process, thereby achieving interfacial enhancement. Although these methods effectively improve the overall performance of rubber composites. Unfortunately, most current studies still have a common problem. The introduction of organic reagents and complex processes not only poses potential environmental hazards but also essentially conflicts with the tire industry's demand for a green transformation. How to construct an efficient interfacial enhancement mechanism while avoiding environmental burdens has become the key to restricting the development of high-performance green tire materials.

In this study, the enhanced interface between GO and NR was constructed through a synergistic enhancement strategy of charge regulation and flexible bridge. A biocompatible cationic polymer, poly (diallyldimethylammonium chloride) (PDDA), was selected as the the modifier for GO. This strategy could not only construct positively charged GO fillers through electrostatic self-assembly. This facilitated the formation of a stable charge adsorption system between GO and anionic NR latex, which addressing the stratification issue caused by density differences in conventional blending processes. More importantly, the non-polar molecular chains within PDDA could form flexible bridge connections with NR during high-temperature mixing. This facilitated the development of a flexible bridging interface between the GO and NR systems. This dual-enhancement mechanism significantly improved the dispersion of GO in the NR matrix and the interfacial interaction. As expected, the prepared NR composites exhibited significantly enhanced mechanical properties and reduced rubber compression fatigue heat generation. This method not only offers new perspectives for the preparation of high-performance and environmentally friendly rubber materials, but also opens up new avenues for the development of low-energy-consumption and long-life green tires.

2. Materials and methods

2.1 Materials

Natural latex (NRL, 60 wt.%) was purchased from Three Trees Co., Ltd. Graphene oxide dispersion (GO, 10 mg/mL) was provided by Changzhou Sixth Element Co., Ltd. Poly (diallyldimethylammonium chloride) (PDDA), anhydrous calcium chloride ($CaCl_2$), N-cyclohexylbenzothiazole-2-sulfenamide (CZ), zinc oxide (ZnO), poly(1,2-dihydro-2,2,4-trimethylquinoline) (RD) and stearic acid (SA) were supplied by Aladdin Reagents Co., Ltd. Carbon black (CB, N330) was provided by Cabot Corporation. Antioxidant 4020 and sulfur were industrial-grade products.

2.2 Preparation of PDDA@GO (PGO) filler

The PGO fillers were prepared through a green and convenient one-pot method. The detailed preparation process was shown in Fig. 1. Firstly, different amounts of PDDA (0.25, 0.35, 0.45 g) were dispersed in water and subjected to ultrasonic treatment to obtain a 2 wt.% PDDA aqueous dispersion. Then, a 2 mg/mL GO aqueous dispersion with a mass of 0.5 g was added to the PDDA aqueous dispersion, followed by continuous ultrasonic treatment for 20 min. Subsequently, the mixture was stirred magnetically at room temperature for 2 h to obtain the PGO dispersion. After centrifugation and multiple washings, the PDDA@GO fillers were obtained by freeze-drying. The mass ratios of GO to PDDA were 0.5:0, 0.5:0.25, 0.5:0.35 and 0.5:0.45, and the fillers were denoted as

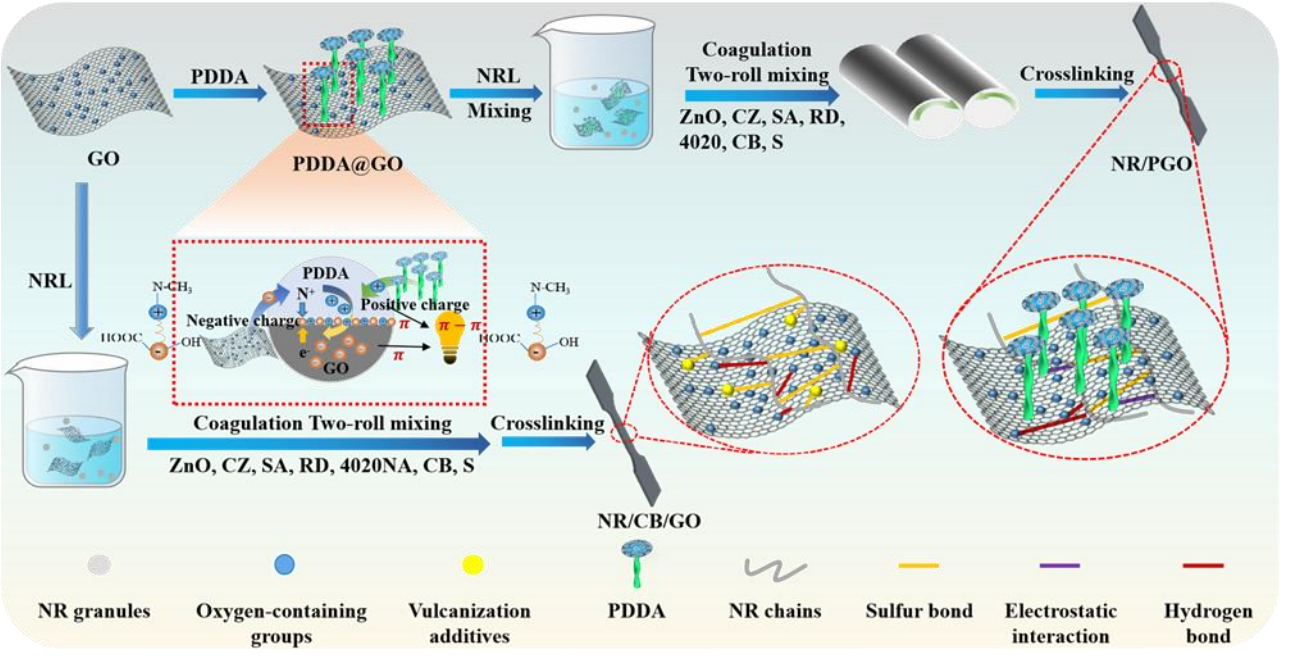

Fig. 1: Schematic diagram of the preparation process of NR/GO and NR/PGO composites.

GO, PGO-25, PGO-35 and PGO-45, respectively.

2.3 Preparation of NR/PGO composites

The NR/PGO composites were prepared through a water-phase co-precipitation process and a hot-press vulcanization process. Firstly, a certain amount of PGO dispersion was added to 30 wt.% diluted NRL for mixing, accompanied by stirring for 30 min. Subsequently, a 10 wt.% $CaCl_2$ solution was added to the mixed emulsion until complete coagulation. The coagulated rubber was then soaked and pressed, and dried in a 60 ℃ forced-draft oven for 16 h to obtain the NR/PGO masterbatch. Finally, the NR/PGO masterbatch was milled using an internal mixer at 110 ℃ and a two-roll mill at 60 ℃. During this process, vulcanization accelerators and reinforcing agents were added sequentially to the masterbatch for thorough mixing. It was noteworthy that, to facilitate the comparison of performance differences between NR/PGO and NR/GO, CB was not added to NR/PGO during the property testing stage; however, 35 phr CB was incorporated into NR/PGO during the solid tire testing, so that the performance of NR/PGO in tires could be of reference value. After the milled rubber was left to stand for 24 h, it was placed in a mold and vulcanized at 150 ℃ and 15 MPa for a certain period of time (Tc90, obtained by RPA) to produce the NR/PGO composites. The NR/PGO composites were denoted as NR/PGO-25, NR/PGO-35 and NR/PGO-45 based on the amount of PDDA added. The specific rubber vulcanization formulations were shown in Table S1.

2.4 Characterizations

The zeta potentials of GO, PGO, and the NR/GO, NR/PGO emulsions were measured using a Malvern Zetasizer Nano-ZS (Malvern Instruments, UK). Prior to testing, a 0.25 mg/mL sample dispersion was prepared by ultrasonic treatment for 10 min. The interaction between GO and PDDA was analyzed using a UV-vis spectrophotometer (Cary 5000, Agilent Technologies, USA) in the wavelength range of 190 nm-900 nm. The crystalline structures of GO and PGO fillers were characterized using an X-ray diffractometer (XRD, 2700B, Haoyuan, China). A Cu target Kα radiation (λ = 0.1546 nm) was used as the source, with the tube voltage and current set at 50 kV and 30 mA, respectively, and the measurement was conducted over an angular range of 5-90°. The interlayer spacing of GO was calculated using Bragg's equation ($\lambda=2d\sin\Phi$). The groups of GO and PGO fillers were characterized using an Invia Raman spectrometer (Renishaw, UK) with an Ar^+ laser (wavelength 514.5 nm). The surface chemical composition and changes in chemical states of different fillers were analyzed using an X-ray photoelectron spectrometer (XPS, NEXSA, Thermo Fisher, USA). The X-ray beam spot size was 400 μm, and the scanning mode was CAE. The pass energy for full-spectrum scanning was 160 eV, and narrow-spectrum scanning was 40 eV. The mass loss of GO, PDDA and PGO fillers was tested using a Q50 thermogravimetric analyzer (TA, USA). Prior to testing, the samples were dried at 60 ℃ for 12 h. The test was conducted in a N_2 atmosphere with a heating rate of 10 ℃/min from room temperature to 800 ℃. The morphology and microstructure of different fillers and NR rubber composites were analyzed using a field-emission scanning electron microscope (SEM, SU8010, Hitachi, Japan) at an acceleration voltage of 15 kV. Prior to testing, the fillers were diluted with ethanol and dropped onto a silicon wafer. After the ethanol evaporated, they were attached to a conductive adhesive. The rubber composites were fractured in liquid nitrogen and the fracture surface was exposed on the outside of the conductive adhesive

for observation. The vulcanization characteristics of NR/GO and NR/PGO composites were tested using an RPA-8000-H rubber processing analyzer (Gotech, China). The dispersion fillers in the NR matrix were observed using a DGAV-SR filler dispersion analyzer (Alpha, USA). Prior to testing, the samples were cut into smooth surfaces with a special knife and placed in the observation window of the analyzer. The dispersion state was characterized by dispersion degree and aggregate size. A differential scanning calorimeter (DSC, DSC-1, Mettler Toledo, Switzerland) was used to analyze the interfacial interactions between different GO fillers and the NR matrix by measuring the glass transition temperature (T_g) of NR composites. The test was conducted in a N_2 atmosphere, cooling from room temperature to -80 ℃ at a rate of 5 ℃/min, and then heating to 25 ℃ at the same rate. A RH-3000 N rubber fatigue compression heat generation tester (Gotech, China) was used to record the compression fatigue heat build-up values of different NR composites at 55 ℃ and a frequency of 30 Hz. Prior to testing, the samples were vulcanized into cylinders with a diameter of 17.8 mm and a height of 25 mm. The mechanical properties of NR composites were tested using an AL-7000 universal tensile testing machine (Gotech, China) at a testing rate of 500 mm/min. The abrasion resistance of NR composites was obtained using a DIN abrasion tester (Gotech, China). The dynamic mechanical properties of NR/GO and NR/PGO were tested using a DMA 850 (TA, USA). the rolling resistance and dynamic temperature rise of NR/GO and NR/PGO prepared as test specimen wheels were measured using a rolling resistance tester (Gotech, China). The crosslink density and bound content of rubber were measured using the toluene equilibrium swelling method.

3. Results and discussion

3.1 Characterization of PGO

The positively charged PDDA was introduced into the GO aqueous dispersion system using ultrasonic-assisted dispersion.[31] Although the surface of GO exhibited negative charge due to the presence of oxygen-containing functional groups such as carboxyl groups, the introduction of PDDA still maintained the good dispersion state of the system. The adsorption of PDDA onto GO was primarily driven by strong electrostatic attraction, further stabilized by hydrogen bonding between the -NH_3 groups of PDDA and the oxygen groups of GO, as well as π–π stacking interactions. The mechanism was illustrated in Fig. 2a.

To verify the electrostatic assembly behavior between PDDA and GO, zeta potential measurements were employed to investigate the surface charge characteristics of GO, PGO and NRL. As shown in Fig. 2b, the pristine GO carried a negative charge. After modification with PDDA, the GO particles exhibited a positive charge, and their surface charge density increased significantly with the addition of PDDA. This was attributed to the higher positive charge density of PDDA compared to the negative charge density of GO, which resulted in incomplete neutralization of PDDA positive charge by GO. Consequently, the PGO particles overall carried the positive charge. This indicated that the PGO particles were successfully obtained via the electrostatic self-assembly of PDDA and GO. Moreover, compared to NRL/GO, the zeta potential of the PGO-filled NRL showed a decrease in the magnitude of the negative charge, which increased with the addition of PDDA. This was due to the electrostatic interactions between PGO and NRL (Fig. S1).

The UV–Vis absorption spectra were employed to further elucidate the interaction mechanism between GO and PDDA, as shown in Fig. 2c. The pristine GO exhibited a maximum absorption peak at 230 nm, corresponding to the characteristic absorption peak of π-π* transition of C=C bonds. After modification with PDDA, PGO showed a significant red-shifted new absorption peak at 237 nm. This was attributed to the π-π conjugation between the double bonds of PDDA and the aromatic rings of GO, which expanded the delocalization range of π electrons and reduced the energy gap between the highest occupied molecular orbital (HOMO) and the lowest unoccupied molecular orbital (LUMO). This indicated the existence of π-π interactions between GO and PDDA.

The microscopic morphologies of GO and PGO were shown in Fig. 2d and Fig. S2. The GO exhibited a tightly stacked and crumpled sheet structure due to van der Waals interactions (Fig. 2d-1), while after modification with PDDA, the GO sheets were significantly exfoliated (Fig. S2, Fig. 2d-2). This was closely related to the structure and properties of PDDA. The surface of GO sheets carried a negative charge due to the presence of a large number of oxygen-containing functional groups such as hydroxyl and carboxyl groups, while the PDDA molecular chains had a significant amount of positive charge. When PDDA was added to GO, the electrostatic attraction between them overcame the van der Waals forces between GO sheets, causing the originally stacked GO sheets to gradually separate. Meanwhile, the certain chain length and volume of PDDA molecules, as well as they could interact with GO via π-π interactions. This prevented the GO sheets from reapproaching each other, and further promoted the separation of the sheets. When the mass ratio of PDDA to GO was 0.35:0.5, the prepared PGO-35 filler exhibited a well-separated sheet structure. However, as the content of PDDA further increased, the excess PDDA molecules entangled with each other, which formed aggregates that created a "bridging" effect between GO sheets. This led to the restacking of GO sheets (Fig. S2d).

The XRD patterns of GO and PGO were shown in Fig. 2e. The pristine GO exhibited a diffraction peak at 12.11°, corresponding to the (001) crystal plane with an interlayer spacing of 0.74 nm. Compared with GO, the diffraction peak of PGO first shifted to the left and then to the right as the content of PDDA increased, which indicated that the interlayer spacing of PGO first increased and then decreased. This was consistent with the results observed by SEM. This indicated that PDDA molecules had successfully intercalated and

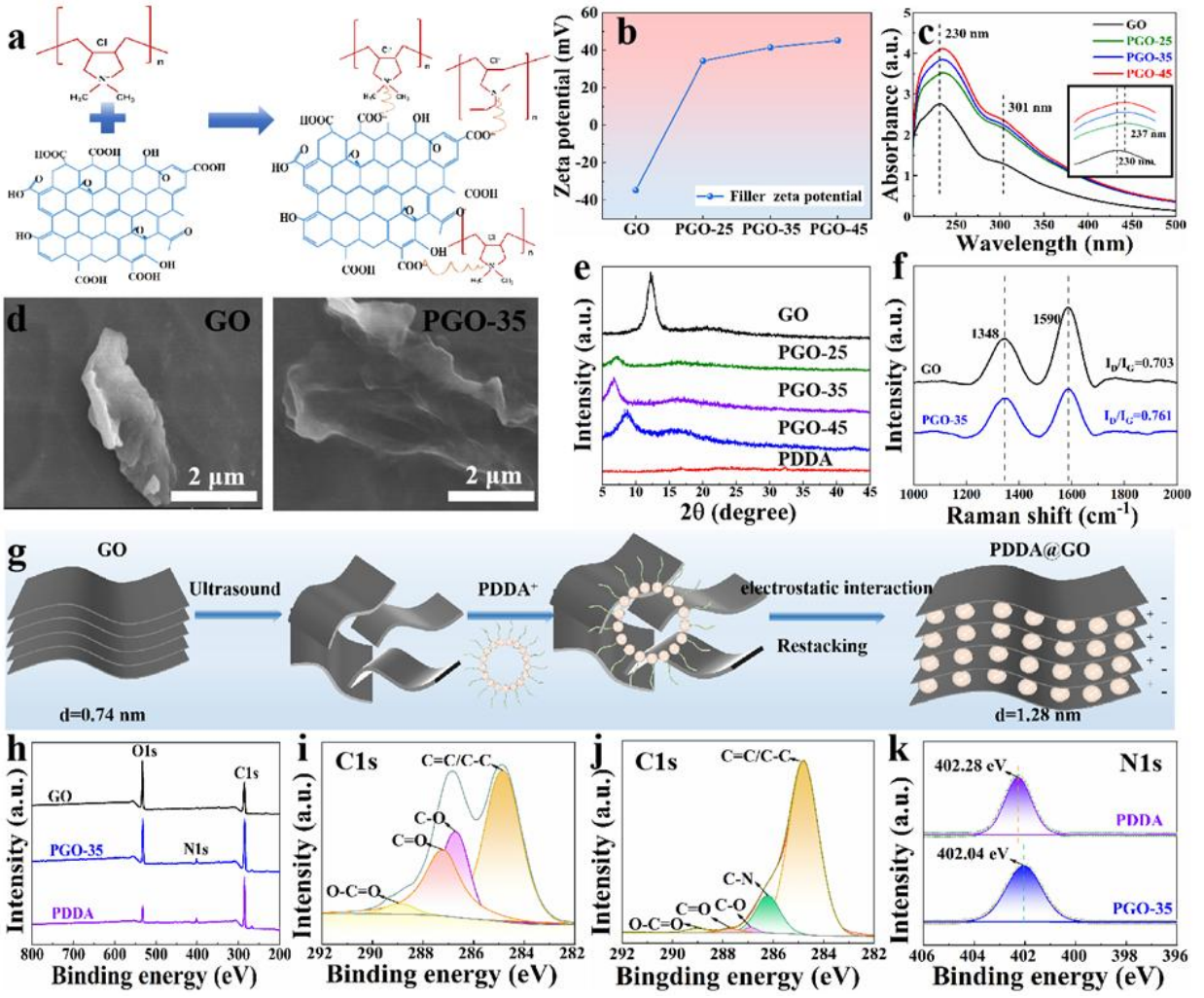

Fig. 2: (a) Schematic illustration of the electrostatic adsorption between GO and PDDA. (b) Zeta potentials of GO and PGO. (c) UV–Vis spectra of GO and PGO. (d) SEM image of GO and PGO-35 fillers. (e) XRD patterns of GO, PGO and PDDA. (f) Raman spectra of GO and PGO. (g) Schematic illustration of the structure formation of PGO. (h) XPS spectra of GO, PGO and PDDA. C1s XPS spectra of (i) GO and (j) PGO. (k) N1s XPS spectra of PDDA and PGO.

exfoliated the GO layers. Since both sides of GO had negatively charged sites, the positively charged PDDA molecules could be inserted between GO sheets under the drive of electrostatic interaction, resulting in an increased interlayer spacing of PGO. When the mass ratio of PDDA to GO was 0.35:0.5, the interlayer spacing of the prepared PGO-35 could reach 1.28 nm. However, when the content of PDDA further increased, the interlayer spacing decreased due to the restacking of GO sheets caused by the entanglement of excess PDDA molecules.

Fig. 2g showed the Raman spectra of GO and PGO particles. The characteristic peaks located at 1348 cm^{-1} and 1590 cm^{-1} corresponded to the defects associated with sp^3 carbon atoms (D-band) and sp^2 carbon atoms (G-band), respectively. Compared with the spectrum of GO, the (I_D/I_G) ratio of PGO increased from 0.703 to 0.761. This indicated that structural defects or increased disorder were introduced during the modification of GO with PDDA. This further confirmed the successful preparation of PGO fillers. The schematic illustration of the adsorption and intercalation process of PDDA on the GO surface was shown in Fig. 2f. It was worth noting that due to the intercalation structure formed between PDDA and GO, the peaks of PDDA itself might become less distinct.

The XPS spectra characterized the surface chemical composition of GO, PDDA and PGO, as shown in Fig. 2h. Compared with pristine GO, the PGO modified with PDDA clearly showed the N1s peak originating from the PDDA polymer at 400 eV. This indicated the successful preparation of PGO. From the C1s peak fitting of GO and PGO (Fig. 2i-2j), it could be seen that the characteristic peaks of C=O and O-C=O in GO were located at 286.8 eV and 288.5 eV, respectively. The C1s spectrum of PGO showed a new peak at 286.1 eV, which was attributed to the C-N bond in PDDA. Moreover, the binding energies of C=O and O-C=O in GO shifted from 286.8 eV and 288.5 eV to higher values of 287.6 eV and 290.1 eV, respectively. This implied a decrease in electron density, likely due to the electrostatic interaction between PDDA and GO.[32] Fig. 2k showed the XPS N1s spectra of PDDA and PGO. The main peak of the N1s

spectra of PDDA and PGO. The main peak of the N1s spectrum of PDDA was observed at 402.28 eV, corresponding to nitrogen-containing substances. When GO was modified with PDDA, the binding energy of this peak decreased by 0.24 eV. In addition, the elemental compositions of PDDA and PGO are presented in Table S2. This suggested that there was a charge transfer from GO to PDDA. The quaternary ammonium groups along the PDDA polymer backbone had a strong electron-withdrawing ability, which allowed them to form electrostatic interactions with the oxygen-containing groups on GO.

The TG and DTG curves of GO, PGO and PDDA were shown in Fig. S3. The thermal decomposition of GO mainly consisted of three stages. The thermal decomposition before 150 ℃ was primarily due to the evaporation of water adsorbed on the GO sheets. The weight loss before 300 ℃ was attributed to the decomposition of unstable oxygen-containing groups on GO. The weight loss in the third stage was due to the thermal decomposition of unstable carbon rings on GO. From the DTG curve, it could be seen that the thermal decomposition of PDDA mainly occurred between 250 ℃ and 500 ℃. Compared with GO, PGO had two main stages of weight loss. The thermal decomposition caused by the unstable side groups of the PDDA main chain occurred between 250 ℃ and 420 ℃. The second stage appeared between 430 ℃ and 500 ℃, which was caused by the thermal decomposition of the PDDA carbon chain backbone. By calculating the residual carbon mass of GO and PGO, the grafting rate of PDDA on GO could be determined to be approximately 21.34%.

3.2 Morphologies of NR/PGO composites

In contrast to the dispersion stability of GO and NRL, which was maintained by electrostatic repulsion, the dispersion of PGO in NR could be divided into two stages. The first stage was the electrostatic-driven pre-dispersion stage. Positively charged PGO was anchored onto the surface of negatively charged NRL particles via electrostatic adsorption, resulting in uniform pre-dispersion (Fig. 3a). The second stage involved the entanglement and flexible polymer bridging between the PDDA molecular chains on the PGO surface and the NR molecular chains during the coagulation step (Fig. 3b).

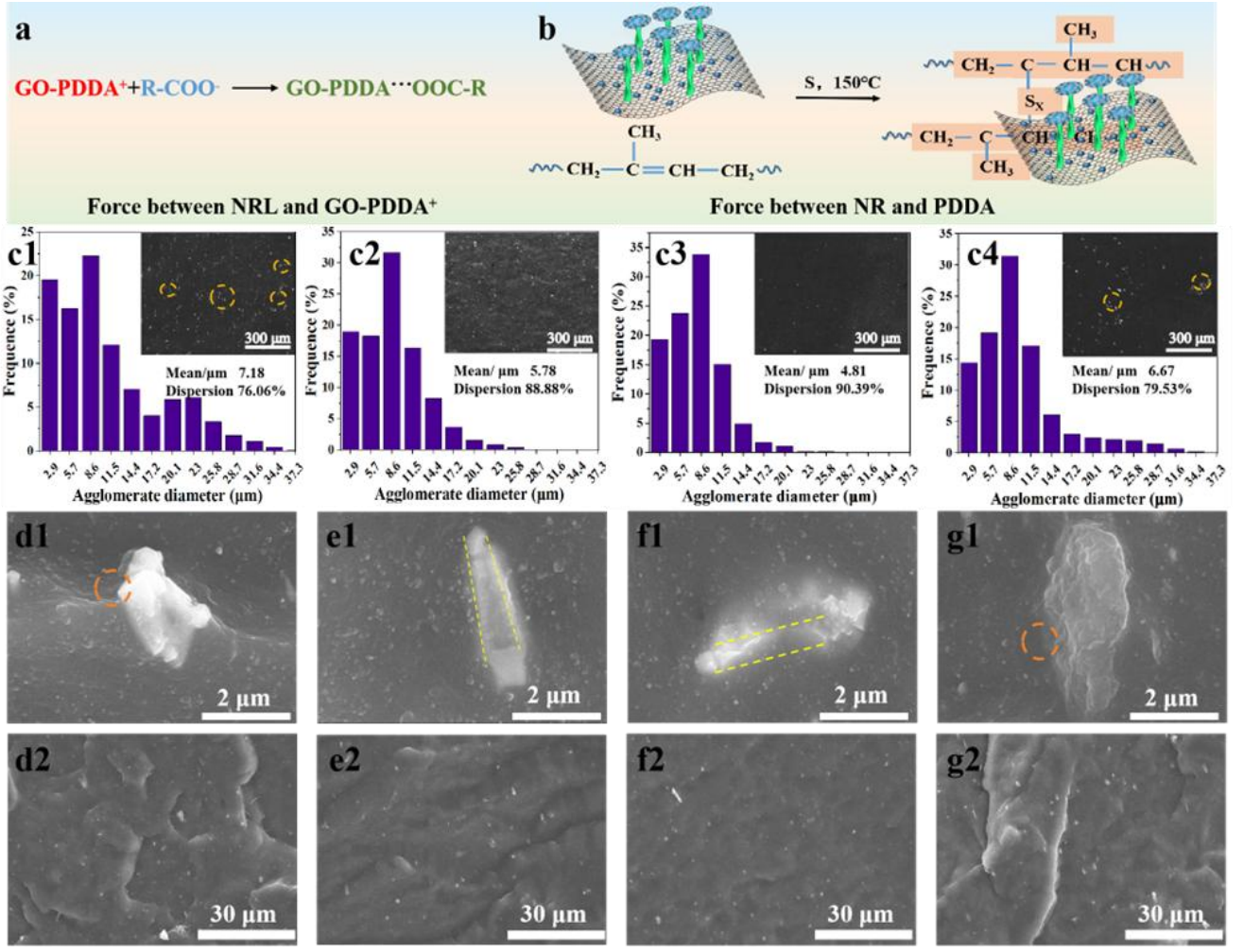

Fig. 3: (a) Schematic illustration of the force between PGO and NRL, (b) Schematic illustration of the force between PGO and NR. (c) Particle size dispersion diagram of NR/PGO and corresponding statistical data ((c-1) NR/GO, (c-2) NR/PGO-25, (c-3) NR/PGO-35, (c-4) NR/PGO-45). SEM images of NR composites ((d-1, d-2) NR/GO, (e-1, e-2) NR/PGO-25, (f-1, f-2) NR/PGO-35, (g-1, g-2) NR/PGO-45).

Throughout the vulcanization process, the PDDA molecular chains became immobilized within the crosslinked network of the NR rubber matrix. This mechanism ensured the long-term stable dispersion of GO within the NR and enhanced interfacial strength.

The filler dispersion within the NR composites was characterized by reinforcing filler particle size analyzer, as presented in Fig. 3c, where white particles denote filler agglomerates.[33,34] It could be observed that the NR/PGO composites exhibited a dispersion characteristic that first improves and then deteriorates with increasing PDDA content, with the NR/PGO-35 composites achieving the best dispersion state. Correspondingly, the agglomerate size also showed a similar trend. In the NR/GO-35 composites, the agglomerates were relatively small, with a size of about 4.81 μm and a dispersion degree of 90.39%. Compared with the NR composites filled with unmodified GO (Fig. 3c-1), the dispersion degree was improved by 18.8%. The phenomenon could be attributed to the intercalation effect of PDDA. PDDA effectively increased the contact area between PGO particles and NRL particles through intercalation into GO, thereby promoting strong binding via electrostatic adsorption. These mechanisms ensured the favorable dispersion of GO filler during the preparation of the NR masterbatch. Furthermore, the enhanced dispersion stability benefited from the flexible polymer bridges formed between the PDDA molecular chains in PGO and the NR matrix. This strengthened the interfacial adhesion between GO and NR and prevented the self-agglomeration of GO filler during the preparation of the vulcanizate. However, excessive PDDA led to its entry into the adsorption layer, resulting in a reduction in electrical double-layer thickness and an increase in ionic shielding effect. This manifested as a decrease in the absolute value of the Zeta potential. Under these conditions, the electrostatic repulsion became insufficient to overcome van der Waals forces, triggering secondary agglomeration of PGO and ultimately causing degradation in the overall dispersion.

The fracture surface of NR/PGO composites was showed in the SEM images (Fig. 3d - Fig. 3g). Obvious GO sheet stacking could be observed in the fracture surface of NR/GO composites, which indicated that the original GO had poor compatibility with the NR matrix. This led to significant GO agglomeration. Compared with NR/GO, the NR/PGO composites showed much finer and more uniform sheet distribution, especially in the NR composites filled with PGO-35(Fig. 3f-2). However, this phenomenon was reversed in the NR/PGO-45 composites (Fig. 3g-1, Fig. 3g-2). This was because excessive PDDA caused GO self-aggregation, weakening the interfacial compatibility between them. The results were consistent with those observed in the filler dispersion. To elucidate potential chemical interactions between PDDA and NR, control samples of NR filled solely with PDDA were prepared. The PDDA-to-NR ratios employed were NR: PDDA = 5:1 and NR: PDDA = 2:1. These formulations excluded both GO and CB while maintaining the standard vulcanization formulation. Analysis of the FTIR spectra (Fig. S4) revealed no characteristic peaks indicative of PDDA participation in the NR vulcanization reaction, demonstrating the absence of chemical crosslinking between PDDA and NR. This finding was consistent with the molecular structure of PDDA and the proposed interfacial mechanism. Consequently, the results confirm that PDDA primarily governs the property enhancement in NR/PGO composites through flexible polymer bridging.

3.3 The crosslinking process and structure of NR/PGO composites

As was well known, in addition to the dispersion of fillers, the interfacial interaction between fillers and the rubber matrix was also a key factor affecting the overall properties of rubber composites. A new interfacial structure was formed between PGO and NR by PDDA, which had a direct impact on the static and dynamic properties of the rubber composites. Fig. 4a showed the vulcanization performance parameters of the NR composites. As the content of PDDA increased, the vulcanization time of the NR composites exhibited a "U" shaped change characteristic. This indicated that the vulcanization rate first increased and then decreased. At the same time, the torque difference (ΔM) also exhibited the same trend (Fig. 4b). ΔM depends on the interaction forces between the filler and the rubber, and it is commonly used to indicate the interfacial bonding strength between the filler and the matrix. It was found that ΔM was relatively high in the NR/PGO-35 composites, indicating that PGO-35 had formed a strong interfacial interaction with NR. This was attributed to the excellent dispersion of PGO-35 filler and its enhanced compatibility with NR. Compared with the unmodified GO-filled NR composites, the PDDA-modified PGO filler exhibited good dispersion due to its altered charge properties. Meanwhile, the PDDA on PGO could participate in the cross-linking of NR molecular chains during the vulcanization stage, acting as a bridge to connect the GO and NR molecular chains. However, when the content of PDDA was too high, the dispersion of GO decreased. This resulted in a decrease in the ΔM value of the prepared NR composites.

From the crosslinking densities (Fig. 4c) and bonded rubber (Fig. 4d) of the NR composites, it was found that the variation trends were observed to be highly consistent. Both parameters were initially found to increase significantly, reaching maximum values, and subsequently decreased with further PDDA addition. This behavior was primarily attributed to the dual influence of PDDA on the filler-rubber interfacial interaction and the crosslinked network structure. At lower PDDA loadings, its molecular chains were able to form flexible bridges through physical entanglement with rubber chains. Simultaneously, PDDA imparted a positive charge to GO, which promoted its combination with negatively charged NR latex particles. These effects synergistically enhanced the filler-rubber interfacial interaction. The enhancement effect was sustained as PDDA content increased to the optimal level.

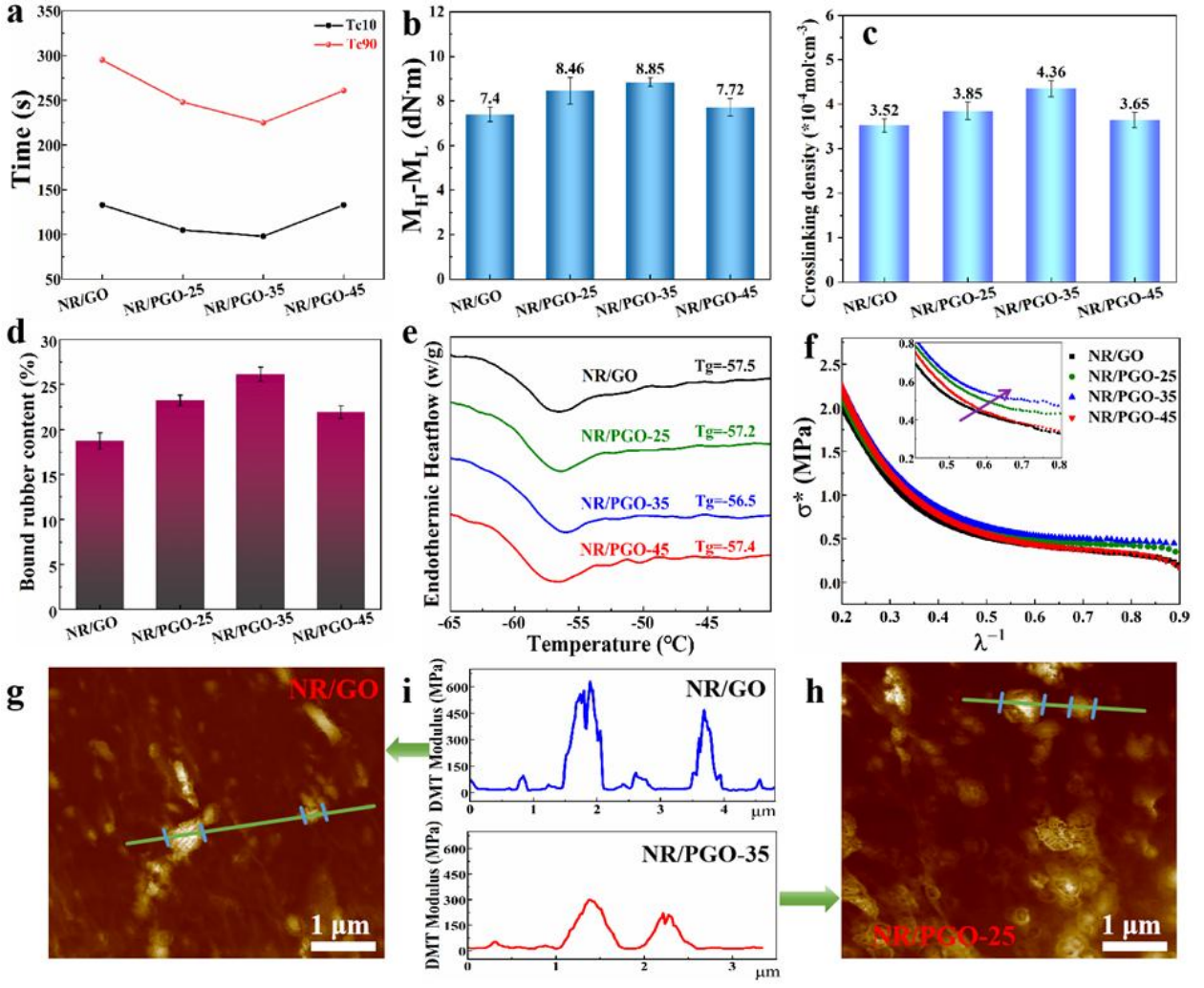

Fig. 4: (a) T_{10}–T_{90} and (b) torque difference (M_H-M_L) vulcanization parameters of the NR/PGO composites. (c) Crosslink density, (d) bound rubber content, (e) DSC curves and (f) Mooney-Rivlin curves of NR composites, (g, h) AFM phase images of NR/GO and NR/PGO-35 composites. (i) The corresponding DMT modulus profiles along the marked lines in (g) and (h).

However, excessive PDDA was found to compress the electrical double layer, leading to the aggregation of GO sheets. This aggregation not only weakened the filler-rubber interface but also reduced the number of effective crosslinking points. This also indicated that PGO-35 filler had better compatibility with NR. A similar phenomenon could also be observed from DSC.

Because the presence of fillers usually causes changes in the glass transition temperature (T_g) of rubber, DSC testing could also be used to measure the extent of interfacial interaction between NR and PGO fillers.[35,36] As shown in Fig. 4e, the NR composites filled with PGO had a higher T_g value than those filled with GO. When the content of PDDA was too high, the T_g shifted to lower temperatures due to the decreased modification effect on GO and the reduced interfacial interaction. This was mainly because the introduction of PDDA formed an ordered molecular layer on the surface of GO, enhancing the interaction between GO and the NR molecular chains. This was because the existence of electrostatic forces between the PGO fillers and the NR macromolecular chains, as well as the increased density of the crosslinking network, restricted the mobility of the rubber chains. This led to an increase in the T_g.

To further analyze the interfacial interaction mechanism of PDDA-modified GO in NR composites, the Mooney-Rivlin model was employed (the details of the Mooney-Rivlin equation were shown in *Supporting Information file*, (Eq. (S1)).[37,38] Fig. 4f presented the Mooney-Rivlin curves of the NR composites. By comparing the degree of upturn of the curves at λ^{-1}, the interaction strength between PGO and NR molecular chains could be quantified. Compared with other NR composites, the inflection point of the NR/PGO-35 composites appeared at a larger λ^{-1} value, which indicated that the NR/PGO-35 composites exhibited strain hardening at a higher stretch ratio. This also reflected a higher stress transfer efficiency at the interface. This enhanced interfacial interaction enabled external forces to be more efficiently transferred into the NR molecular chains, thereby reducing the strain value required to reach the hardening state. This further confirmed that the interaction between PGO-35 filler and NR molecular chains was more pronounced. Therefore, PDDA was demonstrated to exhibit dual functionalities in the

interfacial regulation of NR composites. The interface activation effect was manifested at low load through synergistic enhancement of filler-rubber interfacial binding energy via electrostatic adsorption, which imparted positive charge to GO for improved NR binding. And flexible bridging through physical entanglement forming crosslinking points, significantly improving interfacial adhesion. While the dispersion stabilization effect was achieved by appropriate PDDA content balancing electrostatic repulsion and van der Waals forces between GO sheets to suppress aggregation, thereby ensuring wider and more homogeneous spatial distribution of fillers and consequently reducing inter-filler dynamic friction.

At the nanoscale, AFM DMT modulus mapping (Fig. 4g-i) provided clear evidence of interfacial enhancement. For NR/GO, sharp modulus peaks and narrow interfacial widths (0.58 and 0.30 μm, average 0.44 μm) were observed, together with high RMS fluctuation (135 MPa) and peak modulus values up to 568.6 MPa, indicating heterogeneous interfaces and localized stress concentration. In contrast, NR/PGO-35 exhibited smoother modulus gradients with a slightly larger average interfacial thickness (0.51 μm), much lower peak modulus values (263.4 and 162.6 MPa), and reduced RMS fluctuation (91.4 MPa). These features demonstrate that PDDA modification effectively suppressed filler aggregation, resulting in more homogeneous interfaces and more efficient stress transfer.

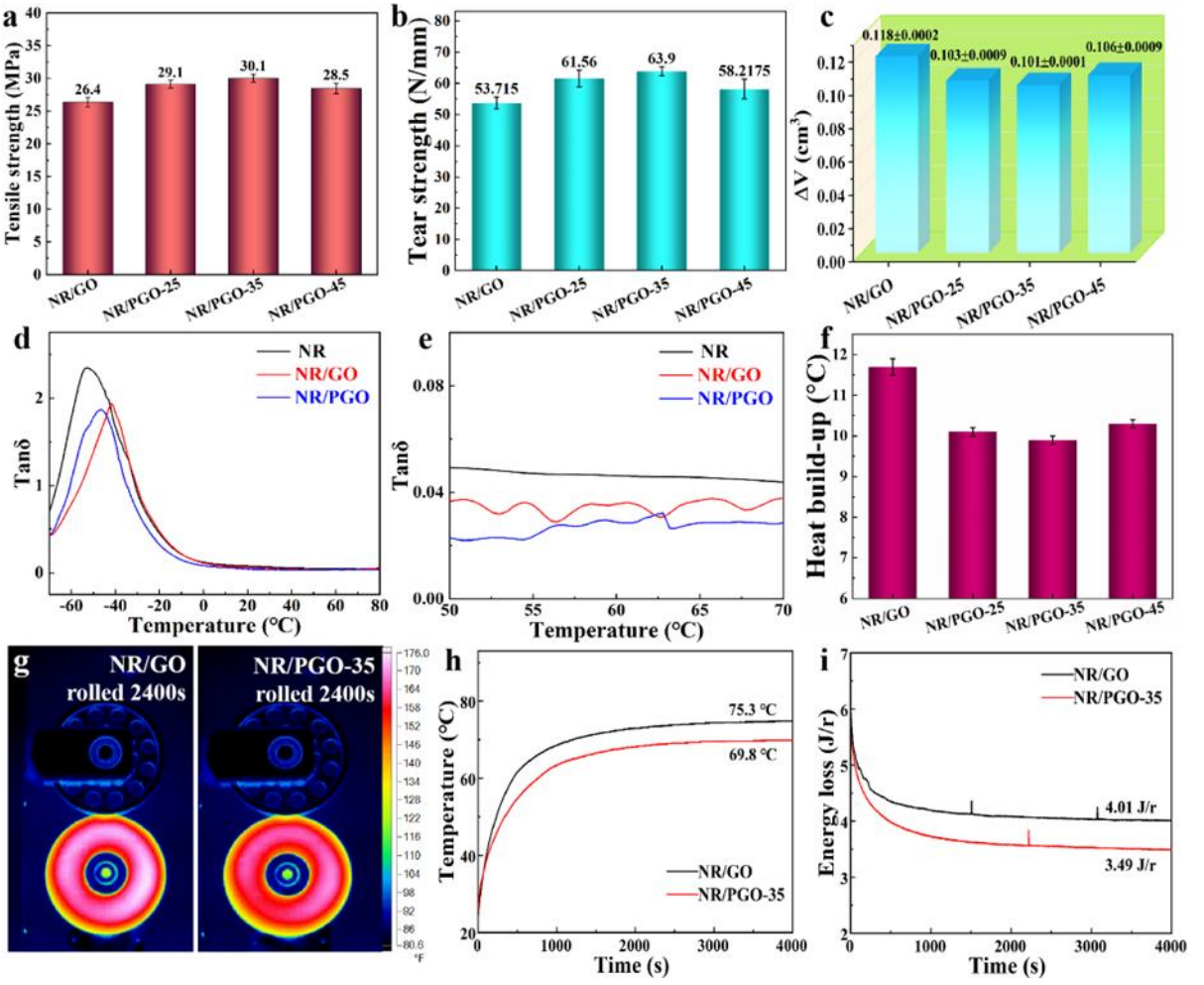

Fig. 5: (a) Tensile strength, (b) tear strength and (c) DIN abrasion of NR/PGO and NR/GO composites. (d) Tanδ - temperature curves and (e) Partial enlarged view of the tanδ - temperature curves near 60 °C for NR/PGO composites. (f) The heat build-up values of NR composites. (g) Infrared thermographic images at 2400 s, (h) temperature rise curves and (i) rolling resistance curves during rolling resistance testing.

3.4 Mechanical properties and tire tread application of NR/PGO composites

The core of green tire design lies in the synergistic enhancement of mechanical and dynamic properties. In this study, the NR/PGO composites prepared using PDDA-modified GO exhibited a significant reinforcement effect on mechanical properties. As PDDA content increased, the tensile and tear strengths of NR composites initially increased and then decreased (Fig. 5a, Fig. 5b). Unmodified NR/GO composites had a tensile strength of 26.4 MPa and a tear strength of 53.7 N/mm. In contrast, the tensile strength of the NR composites filled with PGO-35 could be enhanced to 30.1

MPa, and the tear strength reached 63.9 N/mm, representing increases of 14.0% and 19.0% compared with the NR/GO composites, respectively. Meanwhile, the DIN abrasion test results (Fig. 5c) revealed that the wear volume of the NR/PGO-35 composites decreased from 0.118 cm^3 to 0.101 cm^3, a reduction of 14.4% compared with the unmodified NR/GO composites. In addition to the representative results at 0.5 phr loading, the mechanical properties of NR/GO and NR/PGO-35 at 0.25 phr, 1.0 phr and 1.5 phr were also evaluated (Fig. S5, Table S3). The results showed that NR/PGO-35 consistently exhibits higher tensile and tear strengths, lower DIN abrasion, and reduced heat build-up compared with NR/GO at the same filler contents. Among these, the composites at 0.5 phr demonstrated the most balanced and optimal performance. The improvement in the mechanical and wear resistant properties of NR was attributed to the dual regulation of GO dispersion and interfacial interaction by PDDA. Compared with NR/GO composites, the enhanced flexible bridge interfacial structure of the NR/PGO composites not only reduced the agglomeration and dynamic friction between PGO particles, but also imparted stronger elastic properties to the rubber composite while diminishing some of its viscous characteristics. The most direct manifestation was the improvement in rolling resistance and dynamic thermal properties.

Typically, the rolling resistance of rubber could be represented by the loss factor (tanδ) at 60 °C.[39,40] The lower the tanδ value at 60 °C, the lower the rolling resistance of the rubber composite, and the better the energy-saving effect. As shown in Fig. 5d and Fig. 5e, the NR composites filled with PGO-35 fillers had a relatively low tanδ at 60 °C. This indicated that the use of PDDA as an interfacial modifier for GO and as a bridge for the interfacial connection between NR and GO could effectively increase the elastic modulus of the rubber composite, thereby reducing its rolling resistance at 60 °C. Meanwhile, this also contributed to the reduction of the heat generation during the compression fatigue of rubber.

For rubber used in tire tread compounds, the dynamic thermal properties of rubber are particularly important. Excessive heat generation could lead to thermal degradation of the tread rubber. During the dynamic compression process of rubber, the generation of internal heat originated not only from the friction between rubber molecular chains but also from the friction between fillers and rubber molecular chains, as well as among the fillers themselves. Fig. 5f showed the heat build-up values of different NR composites. Compared with the NR/GO composites, the heat build-up values of NR/PGO composites first decreased and then increased with the increase of PDDA content. The heat build-up values of NR/GO composite was approximately 11.7 °C, while the NR/PGO-35 composites achieved a lower value of 9.9 °C, representing a reduction of about 15.4%. This reduction originated from suppressed friction via improved dispersion and enhanced interfaces.

To thoroughly evaluate the practical application potential of NR/PGO composites, bench testing was employed to simulate tire operating conditions (Fig. 5g). As was well known, the reduction of heat accumulation and rolling resistance, along with the improvement in wear resistance, were considered particularly critical for energy conservation and emission reduction in tires. To this end, NR/PGO and NR/GO solid rubber tires were prepared by vulcanization in molds. A rolling resistance tester was then used to simulate the rolling process of the tires. Under the conditions of a 30 kg load and a rotational speed of 1000 r/min, the heat accumulation and rolling resistance of the two types of tires were compared. The results showed that compared with the NR/GO tire, the dynamic temperature rise of the NR/PGO tire decreased from 75.3 °C to 69.8 °C, a reduction of 7.3% (Fig. 5h). Additionally, the rolling resistance decreased from 4.01 J/r to 3.49 J/r, with an energy-saving efficiency improvement of 13.0% (Fig. 5i). These results indicated that the dual strategies of charge regulation and flexible interface bridging effectively improved the heat generation and energy consumption issues of the tires. The improvements were attributed to the reduced agglomeration and improved dispersion of modified GO, which decreased inter-filler friction. Meanwhile, the increased crosslinking points formed on the filler surface by flexible interface bridging restricted the slippage of NR macromolecular chains, further reducing frictional heat generation between fillers and rubber as well as among rubber molecules. Ultimately, this controlled the heat generation of the tires and significantly enhanced energy-saving efficiency.

4. Conclusion

In summary, this study employed PDDA as a modifier to successfully produce positively charged PGO fillers. Based on the latex co-precipitation method, NR/PGO composites with a dual bonding mechanism were prepared. The PDDA molecules were able to effectively intercalate between the GO layers through electrostatic adsorption and π-π interactions, effectively preventing the aggregation of GO and ensuring good dispersion in NR. This modification strategy not only enhanced the interfacial physical adsorption through the electrostatic interaction between the positively charged PGO and the negatively charged NR latex particles, but also achieved flexible bridge between PDDA and the NR molecular chains during the vulcanization process. This resulted in a dual interfacial bonding mechanism synergistically enhanced by both electrostatic forces and physical entanglement. Benefiting from the good dispersion and strong interfacial interactions, the NR/PGO-35 composites exhibited excellent mechanical and dynamic thermal properties. The tensile strength and tear strength reached 30.1 MPa and 63.9 N/mm, respectively, with improvements in abrasion resistance and dynamic compression heat generation of 13.7% and 15.4% compared with NR/GO composites. More importantly, solid tires prepared from NR/PGO-35 demonstrated lower temperature

rise and rolling resistance, with reductions of 7.3% and 13.0% compared with NR/GO rubber tires. Therefore, the synergistic design strategy of charge regulation and flexible bridge could provide a guidance with both theoretical and practical value for the development of high-performance, energy-saving and energy-efficient tires.

Acknowledgments

The authors gratefully acknowledge the financial support from the Fundamental Research Program of Shanxi Province (202303021212201). This work was also supported by Fundamental Research Program of Shanxi Province (202403021222142), Key R&D Program of Shanxi Province (202302040201007).

Conflict of Interest

The authors declare that they have no known competing financial interests or personal relationships that could have appeared to influence the work reported in this paper.

Supporting Information

Applicable.

CRediT Statement

Shuaishuai Cheng: Conceptualization, Methodology, Investigation, Formal analysis, Writing - Original draft, Project administration. **Bo Xu:** Investigation, Validation, Data curation. **Xiaoyuan Duan:** Software, Resources, Visualization. **Yaqing Liu:** Supervision, Funding acquisition, Writing - Review & editing.

References

[1] E. S. Rødland, G. Binda, D. Spanu, S. Carnati, L. R. Bjerke, L. Nizzetto, Are eco-friendly "green" tires also chemically green? Comparing metals, rubbers and selected organic compounds in green and conventional tires, *Journal of Hazardous Materials*, 2024, **476**, 135042, doi: 10.1016/j.jhazmat.2024.135042.

[2] A. Y. Akhtar, H.-H. Tsang, Dynamic leaching assessment of recycled polyurethane-coated tire rubber for sustainable engineering applications, *Chemical Engineering Journal*, 2024, **495**, 153351, doi: 10.1016/j.cej.2024.153351.

[3] E. Katinas, R. Chotěborský, M. Linda, J. Kuře, Sensitivity analysis of the influence of particle dynamic friction, rolling resistance and volume/shear work ratio on wear loss and friction force using DEM model of dry sand rubber wheel test, *Tribology International*, 2021, **156**, 106853, doi: 10.1016/j.triboint.2021.106853.

[4] S. Yamashita, S. Takahashi, Molecular mechanisms of natural rubber biosynthesis, *Annual Review of Biochemistry*, 2020, **89**, 821-851, doi: 10.1146/annurev-biochem-013118-111107.

[5] Y. Guo, K. Bao, X. Wu, D. Han, J. Zhang, Morphology and aggregation process of natural rubber particles, *Industrial Crops and Products*, 2023, **203**, 117153, doi: 10.1016/j.indcrop.2023.117153.

[6] N. George, C. S. Julie Chandra, A. Mathiazhagan, R. Joseph, High performance natural rubber composites with conductive segregated network of multiwalled carbon nanotubes, *Composites Science and Technology*, 2015, **116**, 33-40, doi: 10.1016/j.compscitech.2015.05.008.

[7] P. Nuinu, C. Sirisinha, K. Suchiva, P. Daniel, P. Phinyocheep, Improvement of mechanical and dynamic properties of high silica filled epoxide functionalized natural rubber, *Journal of Materials Research and Technology*, 2023, **24**, 2155-2168, doi: 10.1016/j.jmrt.2023.03.101.

[8] A. V. Kaliyathan, A. V. Rane, M. Huskic, M. Kunaver, N. Kalarikkal, D. Rouxel, S. Thomas, Carbon black distribution in natural rubber/butadiene rubber blend composites: Distribution driven by morphology, *Composites Science and Technology*, 2020, **200**, 108484, doi: 10.1016/j.compscitech.2020.108484.

[9] L. Zhang, H. Li, X. Lai, X. Liao, J. Wang, X. Su, H. Liu, W. Wu, X. Zeng, Functionalized graphene as an effective antioxidant in natural rubber, *Composites Part A: Applied Science and Manufacturing*, 2018, **107**, 47-54, doi: 10.1016/j.compositesa.2017.12.028.

[10] A. Verma, S. Arora, Enhancement in antimicrobial efficacy and biodegradation of natural rubber latex through graphene oxide/nickel oxide nanoparticles, *International Journal of Biological Macromolecules*, 2024, **265**, 131046, doi: 10.1016/j.ijbiomac.2024.131046.

[11] C. Liu, S. Huang, J. Hou, W. Zhang, J. Wang, H. Yang, J. Zhang, Natural rubber latex reinforced by graphene oxide/zwitterionic chitin nanocrystal hybrids for high-performance elastomers without sulfur vulcanization, *ACS Sustainable Chemistry & Engineering*, 2021, **9**, 6470-6478, doi: 10.1021/acssuschemeng.1c01461.

[12] H. Duan, X. Duan, X. Miao, H. Cheng, C. Liang, G. Zhao, Y. Liu, S. Cheng, Synergistically improving mechanical properties and lowering build-up heat in natural rubber tires through nano-zinc oxide on graphene oxide and strong cross-linked interfaces derived from thiol-ene click reaction, *Advanced Composites and Hybrid Materials*, 2024, **7**, 7, doi: 10.1007/s42114-023-00817-y.

[13] R. Zhang, J. Li, Z. Xu, S. Jerrams, S. Hu, L. Liu, S. Wen, L. Zhang, Achieving strong chemical interface and superior energy-saving capability at the crosslinks of rubber composites containing graphene oxide using thiol-vinyl click chemistry, *Composites Science and Technology*, 2023, **233**, 109907, doi: 10.1016/j.compscitech.2022.109907.

[14] S. Huang, J. Hou, J. Yin, Z. Zhang, B. Ding, Y. Duan, J. Zhang, Anti-blooming effect of graphene oxide on natural rubber latex composite films, *Composites Science and Technology*, 2019, **174**, 142-148, doi: 10.1016/j.compscitech.2019.02.027.

[15] C. Chanal, J. Galipaud, B. Moreaux, J. L. Loubet, P. Sotta, Characterization of oxidative processes associated to low-severity tire tread wear, *Wear*, 2025, **566**, 205753, doi: 10.1016/j.wear.2025.205753.

[16] S. Jitkarnka, B. Chusaksri, P. Supaphol, R. Magaraphan,

Influences of thermal aging on properties and pyrolysis products of tire tread compound, *Journal of Analytical and Applied Pyrolysis*, 2007, **80**, 269-276, doi: 10.1016/j.jaap.2006.07.008.
[17] S. Pang, Y. Yu, L. Zhang, Y. Wu, Adjusting silica/rubber interfacial interactions and properties *via* the click reactions between liquid polybutadiene and silane, *Composites Science and Technology*, 2021, **213**, 108903, doi: 10.1016/j.compscitech.2021.108903.
[18] W. Zhao, J. He, P. Yu, X. Jiang, L. Zhang, Recent progress in the rubber antioxidants: a review, *Polymer Degradation and Stability*, 2023, **207**, 110223, doi: 10.1016/j.polymdegradstab.2022.110223.
[19] X. Zhang, S. Sun, N. Ning, S. Yan, X. Wu, Y. Lu, L. Zhang, Visualization and quantification of the microstructure evolution of isoprene rubber during uniaxial stretching using AFM nanomechanical mapping, *Macromolecules*, 2020, **53**, 3082-3089, doi: 10.1021/acs.macromol.9b02656.
[20] N. Ye, J. Zheng, X. Ye, J. Xue, D. Han, H. Xu, Z. Wang, L. Zhang, Performance enhancement of rubber composites using VOC-Free interfacial silica coupling agent, *Composites Part B: Engineering*, 2020, **202**, 108301, doi: 10.1016/j.compositesb.2020.108301.
[21] D. Wang, Z. Tang, Y. Liu, B. Guo, Crosslinking diene rubbers by using an inverse vulcanised co-polymer, *Green Chemistry*, 2020, **22**, 7337-7342, doi: 10.1039/d0gc02660c.
[22] Y. Li, H. Yang, S. Yu, S. Wu, Z. Tang, B. Guo, D. Wang, H. Ren, M. Tian, L. Zhang, Integrating multiple functional moieties toward environmentally friendly and highly efficient interfacial mediator for rubber/silica composites, *ACS Materials Letters*, 2025, **7**, 425-432, doi: 10.1021/acsmaterialslett.4c02127.
[23] S. Fang, F. Li, J. Liu, L. Zhang, D. Wang, B. Liu, S. Wu, Z. Tang, B. Guo, Rubber-reinforced rubbers toward the combination of high reinforcement and low energy loss, *Nano Energy*, 2021, **83**, 105822, doi: 10.1016/j.nanoen.2021.105822.
[24] S. Wang, Z. Tang, Y. Xiao, D. Wang, B. Guo, L. Zhang, Sulfur co-polymer as a universal adhesive to construct segregated structure in cross-linked rubber toward improved conductive and mechanical properties, *Composites Science and Technology*, 2025, **260**, 110964, doi: 10.1016/j.compscitech.2024.110964.
[25] Y. Liu, Q. Zhou, Q. Lu, C. Han, Z. Zhou, Z. Liang, R. Liu, Y. Nie, Reinforcement and toughening of rubber by bridging graphene and nanosilica, *Journal of Inorganic and Organometallic Polymers and Materials*, 2020, **30**, 337-348, doi: 10.1007/s10904-019-01192-2.
[26] S. Woraphutthaporn, P. Pattananuwat, C. Hayichelaeh, T. Kobayashi, K. Boonkerd, Enhancing the properties of graphene oxide/natural rubber nanocomposite-based strain sensor modified by amino-functionalized silanes, *Polymers for Advanced Technologies*, 2022, **33**, 3386-3398, doi: 10.1002/pat.5789.
[27] B. Zhong, H. Dong, Y. Luo, Antioxidant modified graphene oxide for robust and highly aging resistant rubber composites, *Composites Communications*, 2023, **37**, 101443, doi: 10.1016/j.coco.2022.101443.
[28] L. Chen, X. Guo, Y. Luo, Z. Jia, J. Bai, Y. Chen, D. Jia, Effect of novel supported vulcanizing agent on the interfacial interaction and strain-induced crystallization properties of natural rubber nanocomposites, *Polymer*, 2018, **148**, 390-399, doi: 10.1016/j.polymer.2018.06.058.
[29] B. Zhong, Z. Jia, D. Hu, Y. Luo, D. Jia, F. Liu, Enhancing interfacial interaction and mechanical properties of styrene-butadiene rubber composites *via* silica-supported vulcanization accelerator, *Composites Part A: Applied Science and Manufacturing*, 2017, **96**, 129-136, doi: 10.1016/j.compositesa.2017.02.016.
[30] S. Cheng, X. Duan, Z. Zhang, D. An, G. Zhao, Y. Liu, Preparation of a natural rubber with high thermal conductivity, low heat generation and strong interfacial interaction by using NS-modified graphene oxide, *Journal of Materials Science*, 2021, **56**, 4034-4050, doi: 10.1007/s10853-020-05503-8.
[31] Q. Pei, M. Chen, J. Li, J. Liu, N. Wu, K. Chen, X. Chen, Y. Liu, Y. Feng, G. Ren, X. Liu, The protection of ammonia-oxidizing bacteria (AOB) using PDDA/GO composite materials in high salinity wastewater, *Journal of Water Process Engineering*, 2022, **49**, 102998, doi: 10.1016/j.jwpe.2022.102998.
[32] W. Xue, X. Bo, M. Zhou, L. Guo, Enzymeless electrochemical detection of hydrogen peroxide at Pd nanoparticles/porous graphene, *Journal of Electroanalytical Chemistry*, 2016, **781**, 204-211, doi: 10.1016/j.jelechem.2016.05.036.
[33] J. Liang, Z. Luo, J. Zhong, H. Chen, Effect of silica particle size and coating by natural latex on properties of styrene-butadiene rubber/carbon black/silica composites, *Polymer Composites*, 2025, **46**, 306-320, doi: 10.1002/pc.28988.
[34] M. H. Aghajan, S. M. Hosseini, M. Razzaghi-Kashani, Particle packing in bimodal size carbon black mixtures and its effect on the properties of styrene-butadiene rubber compounds, *Polymer Testing*, 2019, **78**, 106002, doi: 10.1016/j.polymertesting.2019.106002.
[35] D. Florez, S. Hoppe, G.-H. Hu, D. Meimaroglou, Radical bulk polymerization of styrene in the presence of rubber particles from recycled tires: a kinetic study using DSC, *Journal of Thermal Analysis and Calorimetry*, 2021, **143**, 3073-3084, doi: 10.1007/s10973-020-09701-z.
[36] H. Shi, Y. Zhao, Y. Su, S. Hu, Y. Shi, X. Shi, Thermal oxidative aging behavior and lifetime prediction of fluoroether rubber, *Polymer Degradation and Stability*, 2025, **232**, 111106, doi: 10.1016/j.polymdegradstab.2024.111106.
[37] M. Pelliciari, S. Sirotti, A. Aloisio, A. M. Tarantino, Analytical, numerical and experimental study of the finite inflation of circular membranes, *International Journal of Mechanical Sciences*, 2022, **226**, 107383, doi: 10.1016/j.ijmecsci.2022.107383.
[38] Q. Yao, P. Dong, Z. Zhao, Z. Li, T. Wei, J. Wu, J. Qiu, W. Li, Temperature dependent tensile fracture strength model of rubber materials based on Mooney-Rivlin model, *Engineering Fracture Mechanics*, 2023, **292**, 109646, doi: 10.1016/j.engfracmech.2023.109646.
[39] S. Bao, L. Zhu, H. Wang, H. Luo, F. Chen, W. Yu, Z. Zhang, X. Zhuang, Q. Wu, Y. Shangguan, Q. Zheng, Synergistic effect of

compound rubber and SiO_2 nanoparticles on low-temperature toughening and balanced stiffness-toughness of random copolymer polypropylene nanocomposites, *Composites Science and Technology*, 2023, **242**, 110210, doi: 10.1016/j.compscitech.2023.110210.
[40] F. Li, F. Liu, J. Liu, Y. Gao, Y. Lu, J. Chen, H. Yang, L. Zhang, Thermo-mechanical coupling analysis of transient temperature and rolling resistance for solid rubber tire: Numerical simulation and experimental verification, *Composites Science and Technology*, 2018, **167**, 404-410, doi: 10.1016/j.compscitech.2018.08.034.